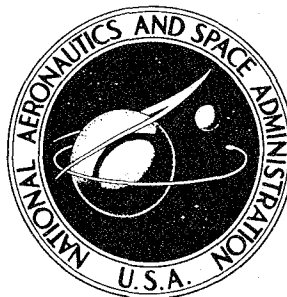


NASA TECHNICAL  
MEMORANDUM



NASA TM X-1330

NASA TM X-1330

19960412 015

PERFORMANCE OF THREE  
ABLATION MATERIALS DURING  
SIMULATION OF LONG-DURATION  
AFTERBODY HEATING

by Marvin B. Dow and Stephen S. Tompkins

Langley Research Center

Langley Station, Hampton, Va.

DISTRIBUTION STATEMENT A

Approved for public release;  
Distribution Unlimited

DTIC QUALITY INSPECTED 1

NATIONAL AERONAUTICS AND SPACE ADMINISTRATION • WASHINGTON, D. C. • JANUARY 1967

REPRODUCED FROM  
PLASTIC FILM COPY OF  
ORIGINAL AERONAUTICS  
RESEARCH REPORT

15596  
9557

PERFORMANCE OF THREE ABLATION MATERIALS DURING  
SIMULATION OF LONG-DURATION AFTERBODY HEATING

By Marvin B. Dow and Stephen S. Tompkins

Langley Research Center  
Langley Station, Hampton, Va.

NATIONAL AERONAUTICS AND SPACE ADMINISTRATION

For sale by the Clearinghouse for Federal Scientific and Technical Information  
Springfield, Virginia 22151 - Price \$2.00

# PERFORMANCE OF THREE ABLATION MATERIALS DURING SIMULATION OF LONG-DURATION AFTERBODY HEATING

By Marvin B. Dow and Stephen S. Tompkins  
Langley Research Center

## SUMMARY

[An experimental investigation was made to determine the resistance to heat penetration and deformations or buckling of three ablation materials during simulated exposure to lifting-vehicle afterbody-heating conditions.] The ablation materials, which were bonded to inconel cones, were subjected to convective heating at cold-wall heating rates ranging from 4 to 40 Btu/ft<sup>2</sup>-sec (45 to 454 kW/m<sup>2</sup>) in arc-jet streams of air and nitrogen. The ablation materials tested were a molded epoxy-based composite and a silicone elastomeric with and without honeycomb reinforcement.

[For the test conditions of the investigation, models with the epoxy-based composite and the unreinforced silicone elastomeric developed buckles in the ablation material; two models of the epoxy-based composite failed catastrophically. The honeycomb reinforcement in the silicone elastomeric was beneficial in restraining thermal expansion and maintaining char integrity.] Except for tests in nitrogen, the silicone elastomerics provided the best resistance to heat penetration.

## INTRODUCTION

Experimental evaluations of the thermal performance of ablation materials are generally performed by testing planar specimens in high-temperature gas streams. Such tests are adequate for obtaining the relative thermal performance of ablative materials, but, because the material boundaries are free to expand during heating, the tests do not simulate the restraints imposed on an ablation material when it is incorporated into the heat-shield system of an actual space vehicle. The coefficient of thermal expansion for an undegraded ablation material may be an order of magnitude higher than that of a metallic substructure and two orders of magnitude higher than that of the degraded ablation material. Therefore, consideration of differential thermal-expansion effects as well as ablative efficiency is necessary in ablative heat-shield design, particularly for the afterbodies of lifting space vehicles. During typical reentry trajectories, the afterbody areas of lifting vehicles will be subjected to long heating times at relatively low heating rates. These heating conditions will cause heat penetration at a faster rate than the

ablation-material degradation and will thus cause differential expansion of the entire heat-shield system. Since the size, configuration, and heating-rate variations of the vehicle afterbody will restrain the thermal expansion, stresses will be produced which might cause premature heat-shield failure or undesirable deformations. These heating conditions and restraints on thermal expansion can be simulated in heating tests of cone models which restrain thermal expansion in the circumferential and longitudinal directions.

The results reported herein were obtained from tests of ablation-material models which were exposed to heating rates and times representative of actual afterbody-heating conditions. Tests were performed in an atmospheric pressure, subsonic arc-jet stream, and, within the operating conditions of the arc-jet, the heating conditions were varied to simulate afterbody heating on a lifting vehicle during an overshoot and an undershoot type of reentry. Three ablation materials were tested on inconel cone models: a molded epoxy-based composite and a silicone elastomeric with and without honeycomb reinforcement. The tests were intended to investigate the ability of the various ablation materials to withstand restrained thermal expansion of the ablation material itself, the integrity at the interface between thermally degraded and undegraded ablation material, differential thermal expansion between the ablation material and the model substructure, and the resistance to heat penetration provided by the different materials. Tests were performed in arc-jet streams of both air and nitrogen to investigate the effect of char-layer oxidation on thermal performance.

During testing, some models experienced severe thermal expansion which caused catastrophic model failure. A picture sequence of one such failure is shown herein. Defects which developed in the various ablation materials are discussed with the aid of photographs. Temperature measurements were made at various locations on the inconel cones, and these measurements provided an indication of the heat-penetration resistance afforded by the different ablation materials.

## SYMBOLS

The units for the physical quantities used herein are given both in the U.S. Customary Units and in the International System of Units (SI). (See ref. 1.) An appendix is included for the purpose of explaining the relationship between these two systems of units.

- a            height of model noscap above arc-jet nozzle, inches or centimeters
- d            diameter of arc-jet nozzle, inches or centimeters

$l$	length of model afterbody, inches or centimeters
$\dot{m}$	mass flow rate of gas through arc-jet nozzle, pounds mass/second or kilograms/second
$Q$	product of cold-wall heat-transfer rate and time, British thermal unit/foot <sup>2</sup> or joules/meter <sup>2</sup>
$q$	cold-wall heat-transfer rate, British thermal unit/foot <sup>2</sup> -second or watts/meter <sup>2</sup>
$t$	time, seconds
$x$	distance along side of cone, inches or centimeters

Subscripts:

$av$	average
$o$	location at $x = 0$ on metal calorimeter
$tot$	total

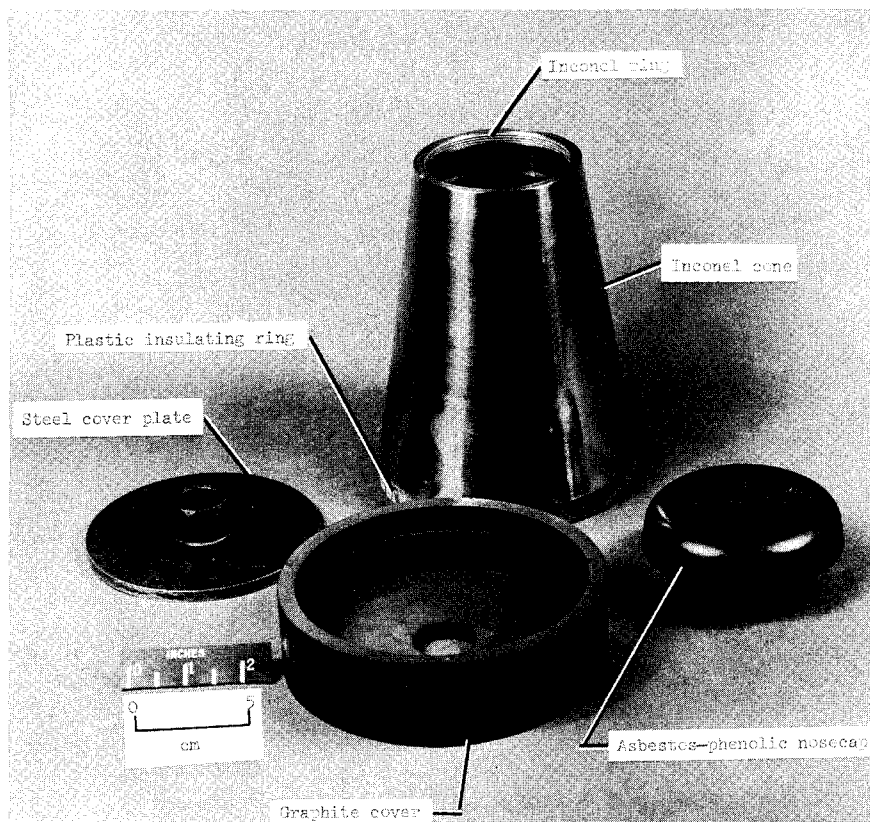
Notation:

$EC$	time at which arc-jet heating rates were changed in trajectory II simulation
$F$	termination of arc-jet heating
$T.C.$	thermocouple
$S$	beginning of arc-jet heating

## TEST MODELS

### Construction

All test model components except the ablation materials were fabricated by the NASA Langley Research Center and are shown in figure 1. The truncated cone, to which the test material was attached, had a half-angle of  $9^{\circ}$  and was constructed of 0.032-inch-thick (0.81-mm) inconel. An internally threaded inconel ring was riveted to the small end of the cone to permit attachment of the nosecap. A large plastic ring was attached by screws to the large end of the cone which provided an insulating attachment to the steel cover plate and thus to the test fixture. A plastic nosecap was machined from asbestos-phenolic and screwed into the small end of the cone to provide a smooth fairing with the test material on the exterior of the cone. The nosecap was thick in order to minimize the heat reaching the inconel cone from the nose region. The nosecap also forced the ablation material to expand longitudinally in the direction of the large end of the cone during heating. The graphite cover fit loosely and served as a fairing between the specimen and the test fixture and also protected the rear of the specimen from heating. For



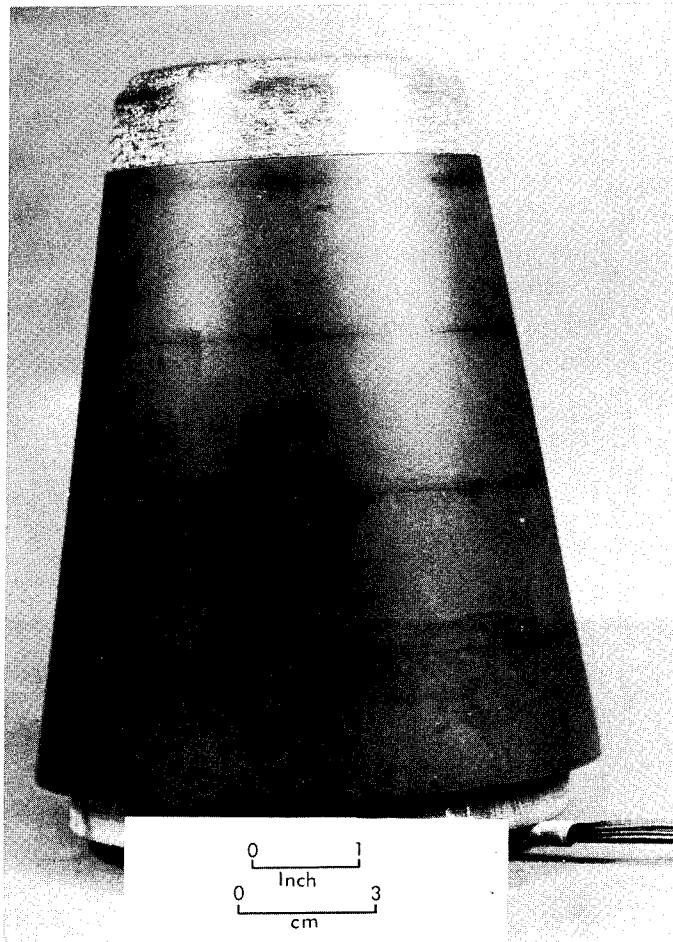
L-62-7825.1

Figure 1.- Supporting structure for ablation material.

Thermocouples were attached at various locations on the inside of the inconel cone, the back of the nosecap, and on the steel cover plate. The locations of these thermocouples are shown in figure 2.

The ablation materials were bonded to the inconel cones by the material suppliers. The fabrication techniques for each ablation material were developed by its supplier. No information is available concerning either the procedure used in the material fabrication





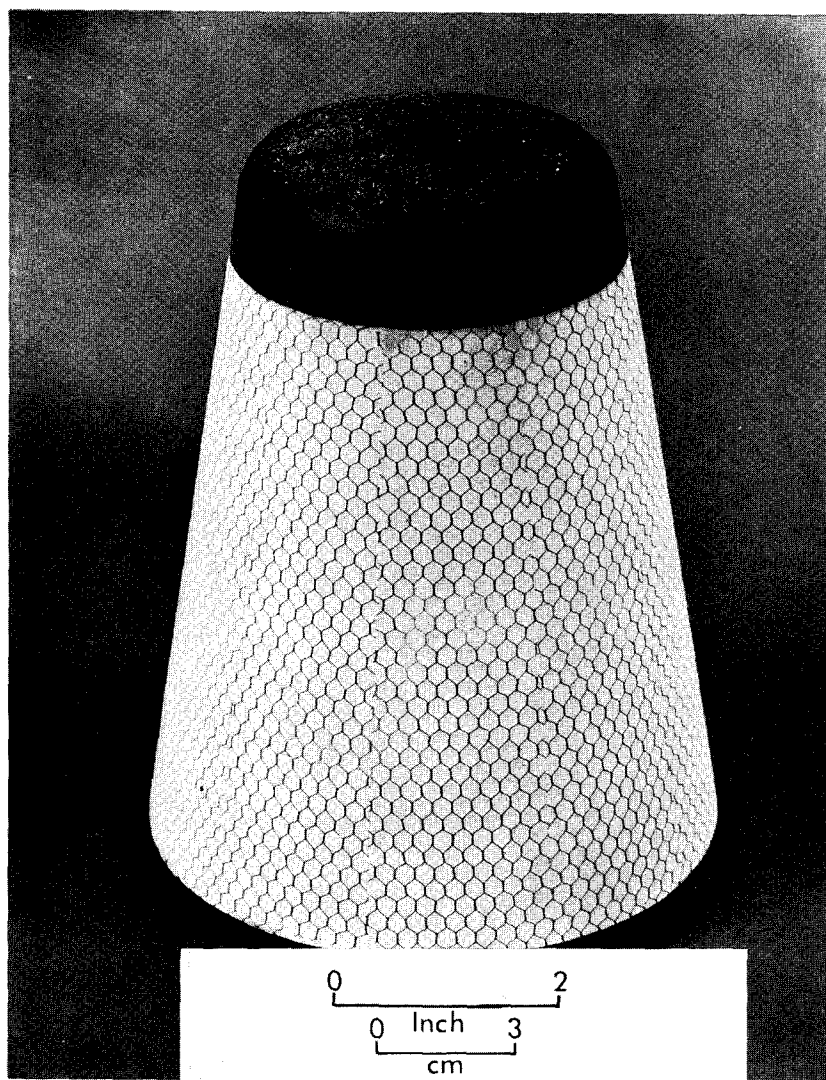
L-62-8160

(a) Material A, epoxy resin filled with phenolic-microballoons and quartz fibers.

Figure 3.- Test specimens.

or the bonding materials and techniques used to bond the ablation material to the inconel cones. General information concerning the ablation materials is summarized in table I. Hereafter, the materials are identified by the letters appearing in table I. Typical pre-test models of each type of ablation material are shown in figure 3. Note that material A was made in rings which were then bonded to the inconel shell.

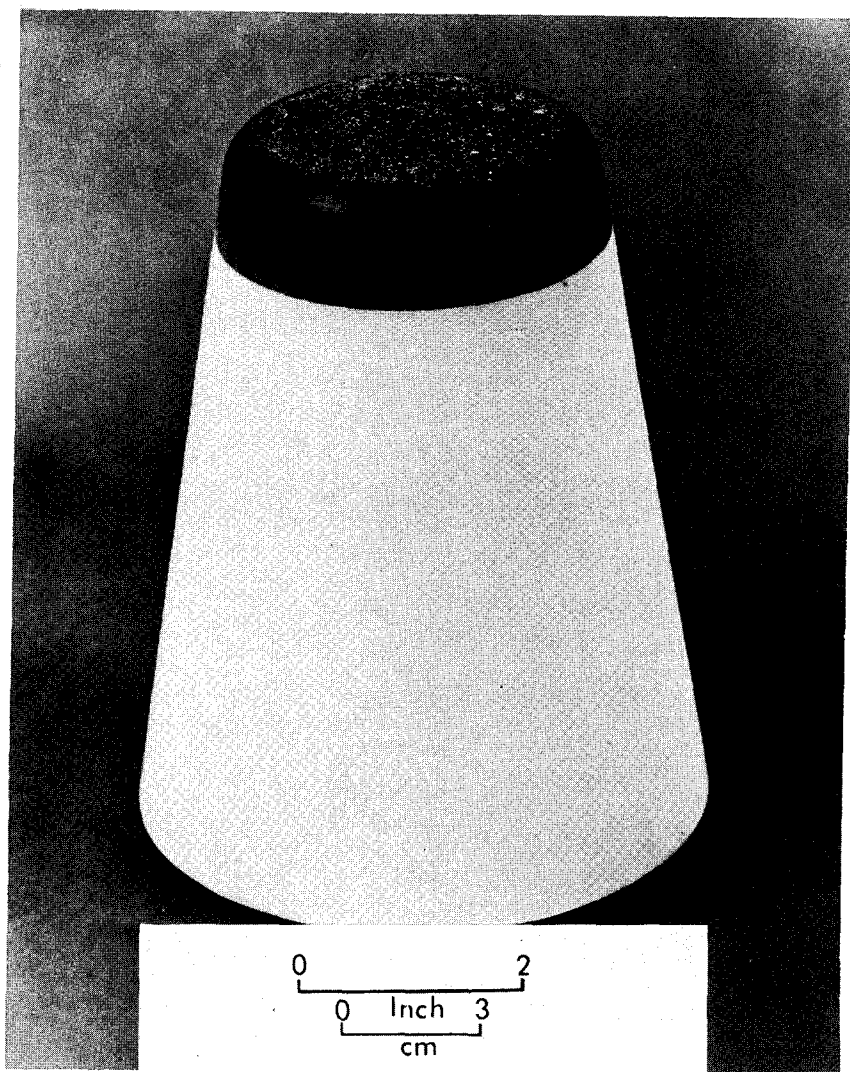
The external model configuration was the largest size which could be tested in the available arc-jet facility. The ablation materials were bonded to the inconel cones in thicknesses equivalent to  $1.5 \text{ lbm/ft}^2$  ( $7.3 \text{ kg/m}^2$ ). This mass per unit area was chosen as representative of afterbody thermal-protection requirements. Greater thicknesses of ablation material were not tested because smaller inconel cones would have been required and because the radii and curvature of the inconel cones used were already considerably different from an actual vehicle.



L-62-7821

(b) Material B, silicone elastomeric and silica spheres in nonmetallic honeycomb.

Figure 3.- Continued.



(c) Material C, silicone elastomeric and silica spheres. L-62-7822

Figure 3.- Concluded.

## TEST APPARATUS, CONDITIONS, AND PROCEDURES

### Test Apparatus

The Langley 2500-kilowatt arc jet was used for testing. Construction and operation details of this facility are presented in reference 2. This facility was the only available facility which could provide the long heating times for the size models used in the present investigation. This facility produces a subsonic gas stream at atmospheric pressure with a static temperature of about  $6800^{\circ}\text{F}$  ( $4000^{\circ}\text{K}$ ). Figure 4 shows the arc jet with a model in testing position.

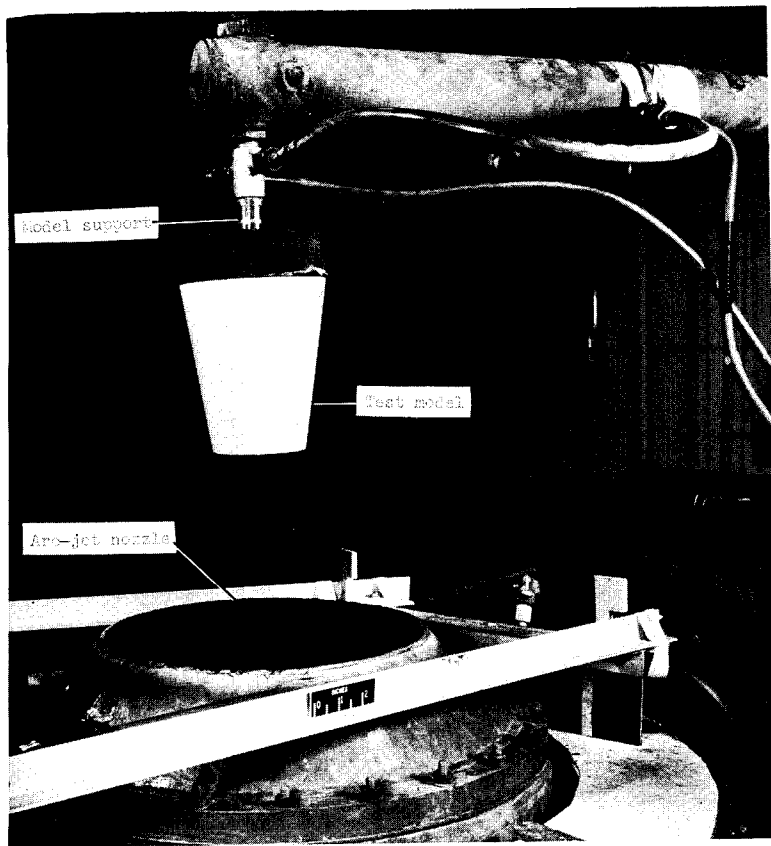
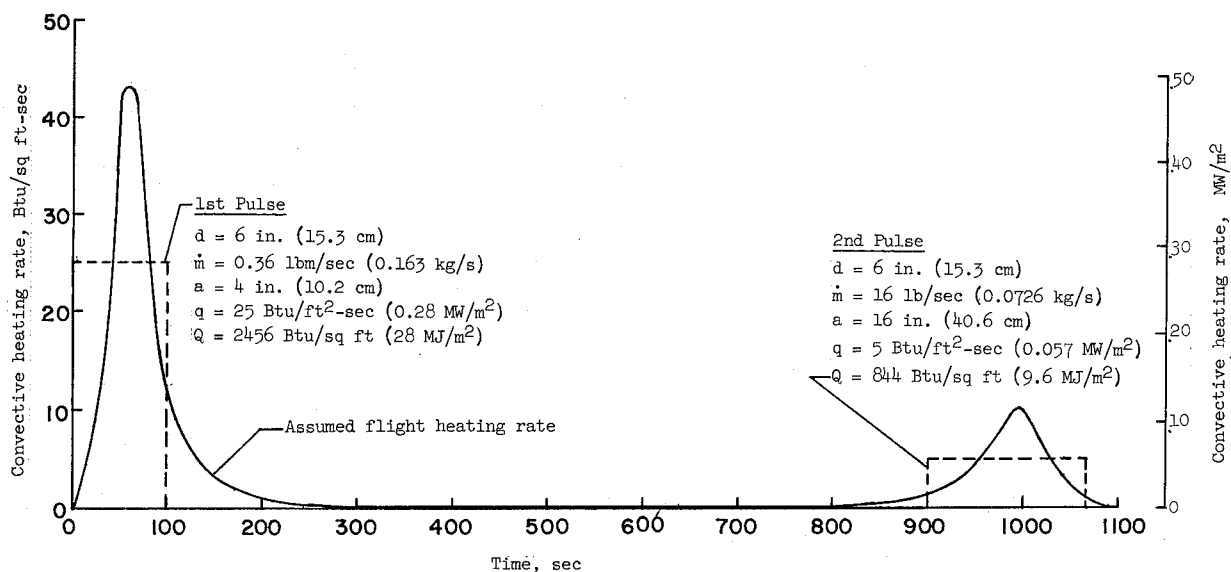


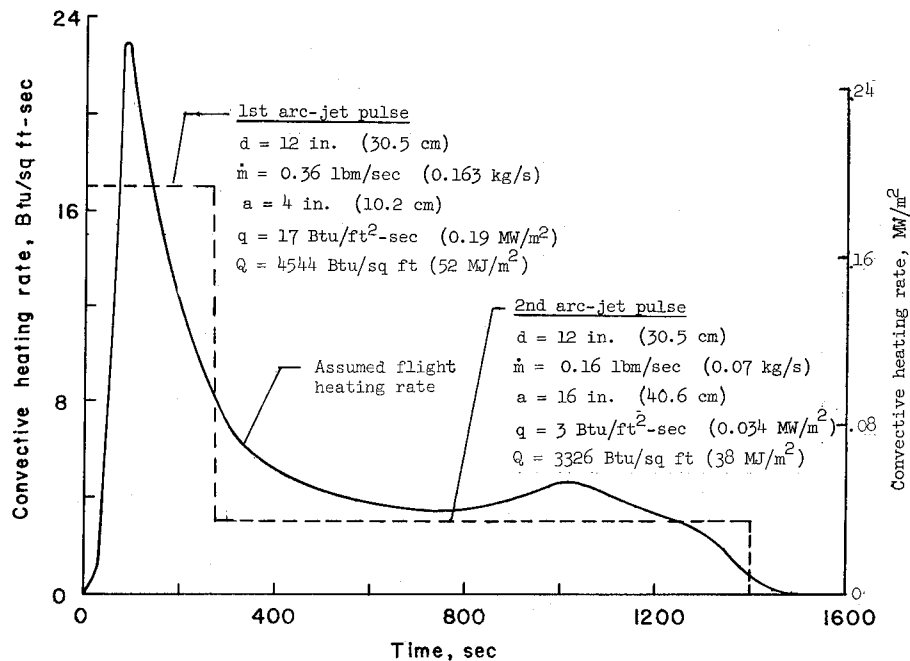
Figure 4.- Test setup. L-63-1799.1

### Test Conditions

The two cold-wall heating-rate histories shown in figure 5 as trajectories I and II were chosen as representative of the heating rates imposed on the afterbody of a lifting vehicle entering the earth's atmosphere at escape velocity. Trajectories I and II represent undershoot and overshoot trajectories, respectively. Each trajectory represents a "skip type" and is characterized by two heating pulses separated by a period of low



(a) Trajectory I.



(b) Trajectory II.

Figure 5.- Assumed flight cold-wall-heating-rate histories and arc-jet simulation. Arc-jet heating rates are  $q_{av}$  at  $x/l = 0.5$ .

heating. Although, in trajectory I, the level of heating is extremely low from 300 to 800 seconds, the heating is continuous throughout the trajectory. Since figure 5 represents afterbody heating, only convective heating is considered. Operating limitations of the arc-jet facility did not permit the heating-rate variations required for duplication of the assumed flight trajectories shown in figure 5. Therefore, both trajectories I and II were simulated by the dashed curves shown in figure 5. The dashed curves are shown as curves of constant cold-wall heating rate which refers to the heating rate to a cold non-ablating wall exposed to the arc-jet stream. The exposure time at each arc-jet heating rate was adjusted so that the area under the dashed curves was equal to the area under the assumed flight heating-rate curves. The arc-jet heating rates were varied by changes in nozzle size, mass flow rate of gas through the nozzle, and the height of the model above the nozzle exit. The arc-jet operating conditions for each heating rate are shown in figure 5.

The arc-jet heating rates shown in figure 5 are an average of the heating rates measured at  $x/l = 0.5$  (fig. 2) with a thin-wall metal calorimeter having the same size and shape as the test specimens. The variations in measured heating rate along the calorimeter for each heating pulse are shown in figure 6.

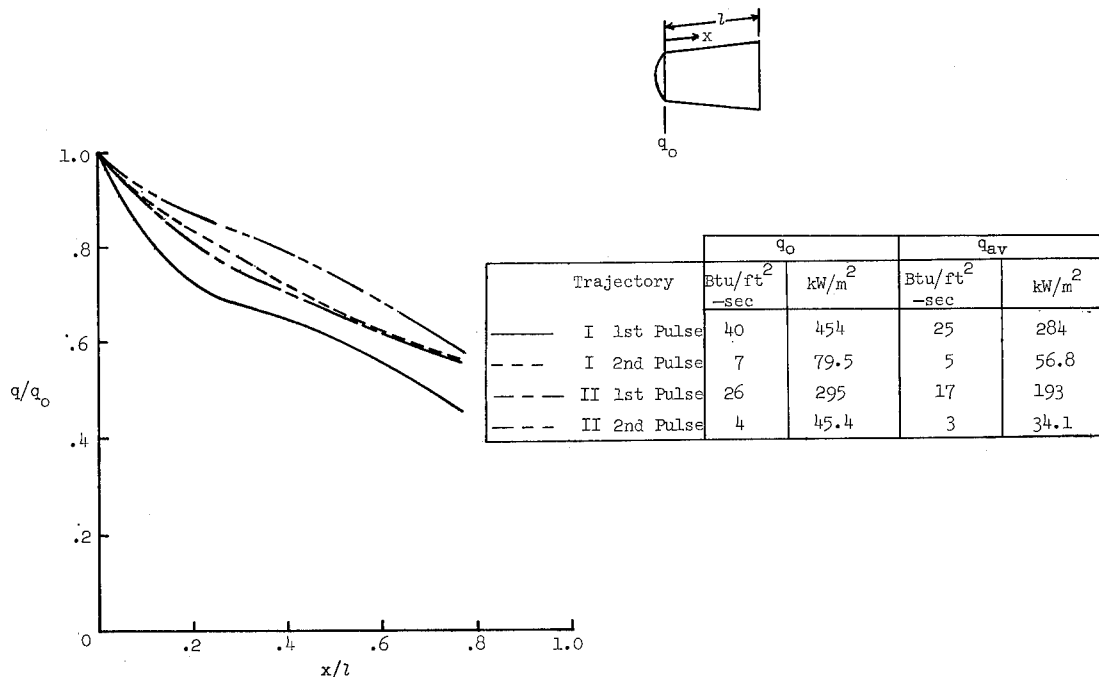


Figure 6.- Cold-wall heating-rate distributions on sides of 90° cone calorimeter.

The available equipment did not permit a determination of stream enthalpy at the various model test positions. The energy-balance values of stream enthalpy at the nozzle exit of both nozzles used in this investigation were 2500 Btu/lbm (5.8 MJ/kg) and 3000 Btu/lbm (7.0 MJ/kg) for the 0.36 lbm/sec (0.16 kg/s) and 0.16 lbm/sec (0.07 kg/s) mass flow rates, respectively. Mixing of unheated surrounding air into the arc-jet stream probably produced a marked decrease in stream enthalpy particularly at the  $a = 16$  inch ( $a = 40.6$  cm) model position. The stream enthalpy at this test position was estimated to be 1000 Btu/lbm (2.3 MJ/kg).

Nitrogen was used for the arc-jet stream in several model tests to determine the oxidation effect on the thermal performance of the ablation material. The results of reference 3 show that oxidation can have a considerable effect on the performance of certain ablation materials in the low-enthalpy arc-jet facility used in the present investigation. Because of surrounding air mixing with the arc-jet stream, some oxygen was present in the nitrogen stream.

### Test Procedures

The procedure for the simulation of trajectory I was as follows: After the arc-jet operating conditions for the first heating pulse were established, the metal calorimeter was inserted into the test stream to obtain a measurement of the cold-wall heating rate for comparison with the values previously measured in establishing the test conditions. After removal of the calorimeter, the model was inserted into the stream for the first heating pulse. At the end of the first heating pulse, the model was removed from the stream and covered with an insulated container. The model was covered to minimize heat losses during the long time between heating pulses since it was not possible to continue heating at the extremely low level required for exact simulation. During the time the model was covered, the necessary changes were made in model height and arc-jet operating conditions required for the second heating pulse. Just prior to the initiation of the second pulse, the insulated container was removed from the model, the arc jet was started, and the calorimeter was employed to obtain a heating-rate measurement. At the proper time, the model was inserted into the arc-jet stream for the second heating pulse. For the trajectory II simulation, the arc jet operated continuously. The heating-rate changes were accomplished by changing the model height and the mass flow of gas without stopping the arc jet. Because of the 12-inch-diameter (30.5-cm) nozzle used for the trajectory II simulation, heating-rate measurements just prior to model insertion could not be made.

## RESULTS AND DISCUSSION

Table II is a summary of the test conditions for each model and shows the arc-jet-stream composition, cold-wall heating rates, and the time of exposure at each heating rate. Models 3 and 4 failed before completion of the simulated trajectory. Figures 7 to 12 show post-test photographs of the various models except for figure 9 which is a photosequence of the model 3 failure. The temperature histories of the model thermocouples are shown in figures 13 to 16.



(a) Model 1 in air. L-63-752

Figure 7.- Material A after trajectory I simulation.

### Appearance of Tested Models

Material A.- Models 1 and 2 are shown in figure 7 after trajectory I simulation. The char layer which formed on this material developed irregular cracks resembling "mud flat" cracks over the entire surface. This crack pattern, which was also observed in tests of planar specimens of this material (ref. 4) was probably due to char shrinkage during degradation. Circumferential buckles which developed during heating are visible in the photographs. Shrinkage of the char layer during cooling after test completion accentuated the larger cracks visible in figure 7.



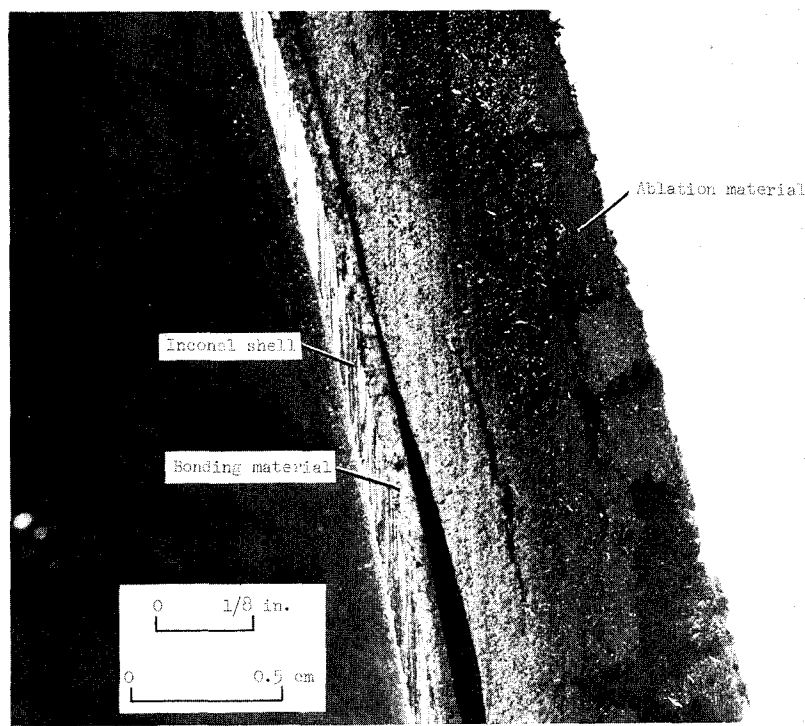
(b) Model 2 in nitrogen. L-63-745

Figure 7.- Concluded.

There is a considerable difference in the appearance of the models tested in air and in nitrogen. It is not known whether the white glassy deposit on the model tested in air was caused by ablation of material A or by deposition of ablation products from the nose cap. The model nose cap material was severely affected by the air test streams as evidenced by the droplets of a glassy material which are visible in figure 7(a), but were not produced in the nitrogen test (fig. 7(b)).

Figure 8 shows a section view of model 2 after testing. The view shown is near the midlength of the model at the location of one of the circumferential buckles previously mentioned. Note that the bonding material adhered to the inconel but that separation occurred at the interface between the bonding material and the ablation material. The buckle encompasses the entire depth of the ablation material. This buckling behavior indicated that the ablation material was not readily able to accommodate restrained thermal expansion; however, the test models had small radii and the ablation materials were severely restrained, and thereby accentuated the thermal-expansion problems. The buckling observed in these tests might not occur on larger models but it is a potential problem area. It is also likely that the behavior of material A is representative of other molded ablation materials of this type, such as low-density phenolic-nylon.

Models 3 and 4 were exposed to the trajectory II simulation in air. Post-test photographs of these models are not shown because the ablation material came off before

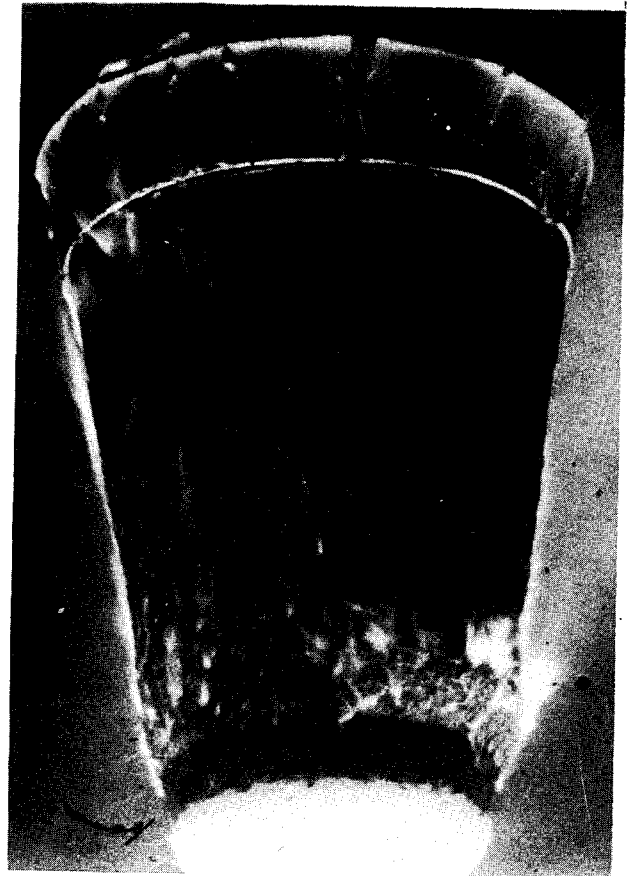


L-63-1903  
Figure 8.- Section view of material A, model 2, after trajectory I simulation.

test completion. Figure 9 shows a sequence from motion-picture film of the failure of model 3. Between 115 seconds and 218 seconds, the buckles gradually increased in severity with failure occurring at 230 seconds. Figure 14(a) shows that the inconel cone temperatures at the initiation of buckling (115 seconds) were about 200° F (367° K). Thus, it seems unlikely that the ablation-material buckling was due to high temperatures in the bonding material. The temperatures on the inconel cone did not reach high values until the ablation material was severely buckled with cracks and holes which permitted hot-gas intrusion. The test of model 4 was a repeat of the model 3 test to determine whether the model failure would be repeated. Model 4 developed the same severe buckles as model 3 during the first heating pulse; however, the ablation material did not fail catastrophically until 336 seconds into the second heating pulse. Motion-picture film of this test showed holes appearing in the buckled material near the end of the first heating pulse. Hot gas entering these holes produced high temperatures on the inconel cone.



(a) Beginning of test  $t = 28$  sec. L-66-7608



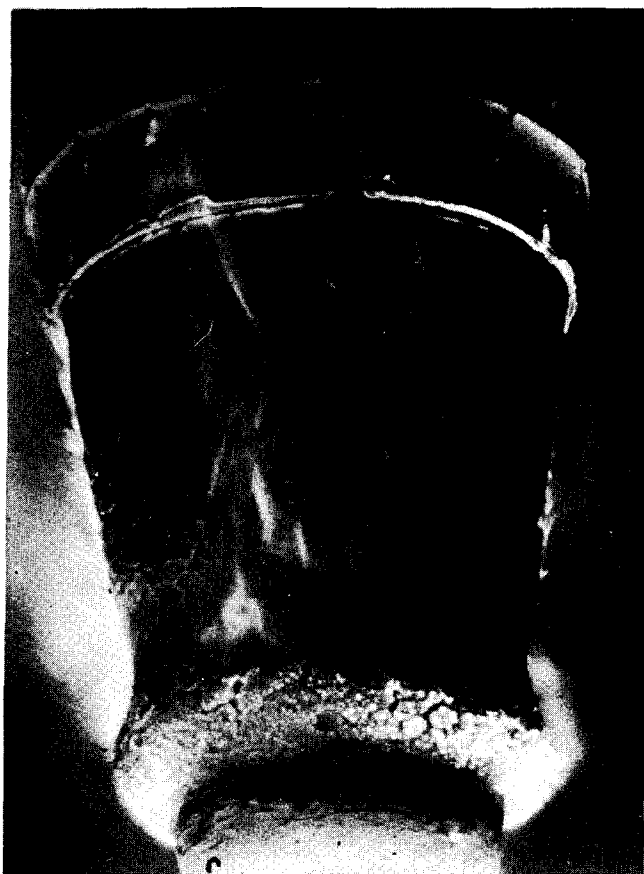
(b) Initiation of buckling  $t = 115$  sec. L-66-7609

Figure 9.- Test of material A, model 3, trajectory II.

The failures of models 3 and 4 were apparently caused by the same buckling behavior observed in models 1 and 2. The longer heating time of the first pulse of trajectory II caused continued growth of the buckles and eventual failure.

Material B.- Post-test photographs of material B models are shown in figure 10. Models 5 and 6 were exposed to the trajectory I simulation in arc-jet streams of air and of nitrogen, respectively. Because of experimental difficulties, the length of time between the first and second heating pulses was longer for model 5 than for the other models exposed to the trajectory I simulation. Material B exhibited a pronounced swelling during testing and increased in thickness by nearly one-third. The increase in thickness is evident in the photographs at the junction of the ablation material and the model nose-cap.

After the trajectory I simulation in both air and nitrogen, the outer surface of the ablation material was covered with a weak friable residue. This residue adhered to the

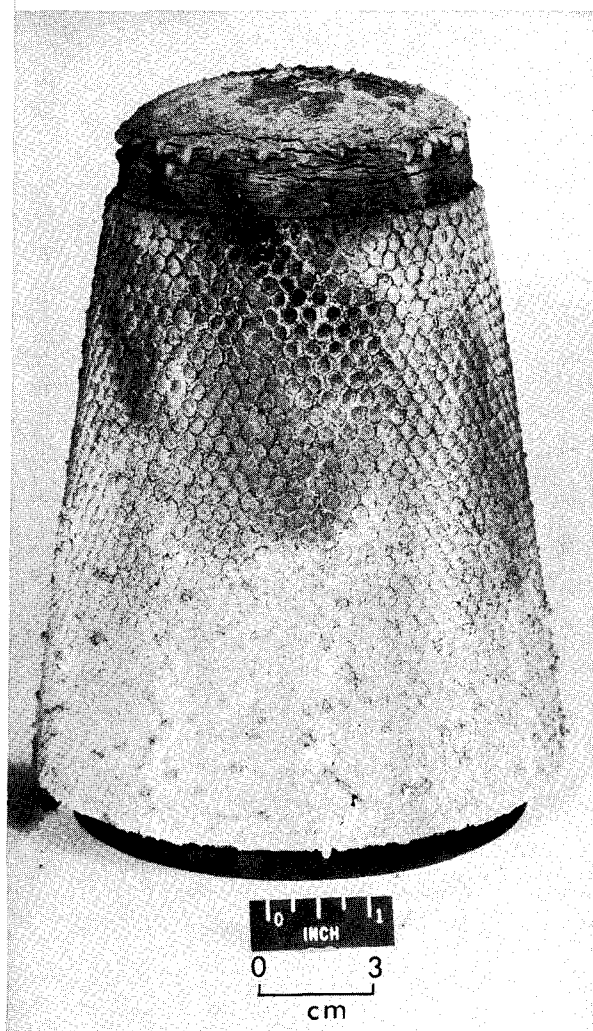


(c) Severe buckling  $t = 218$  sec. L-66-7610

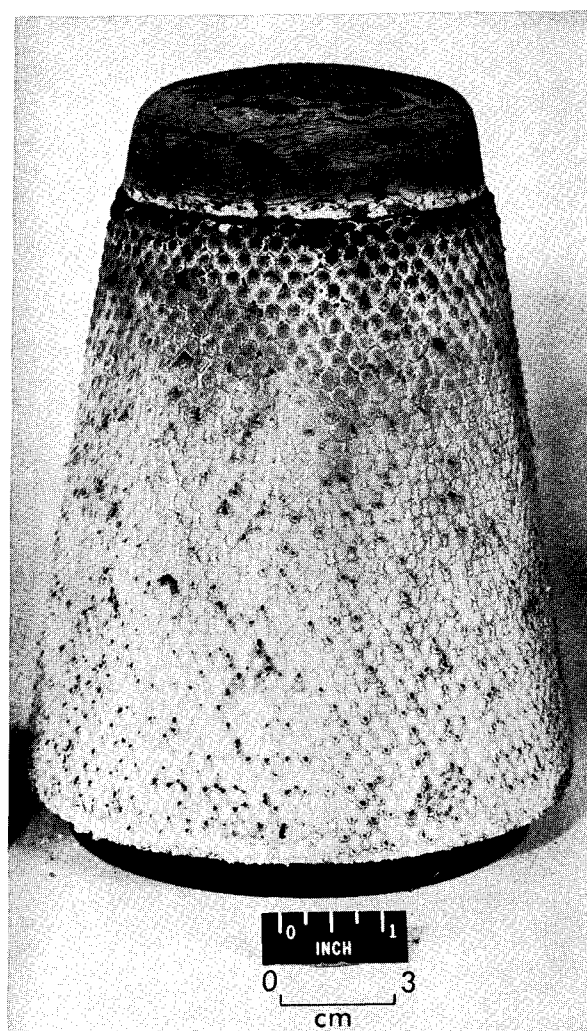


(d) Failure  $t = 230$  sec. L-66-7611

Figure 9.- Concluded.



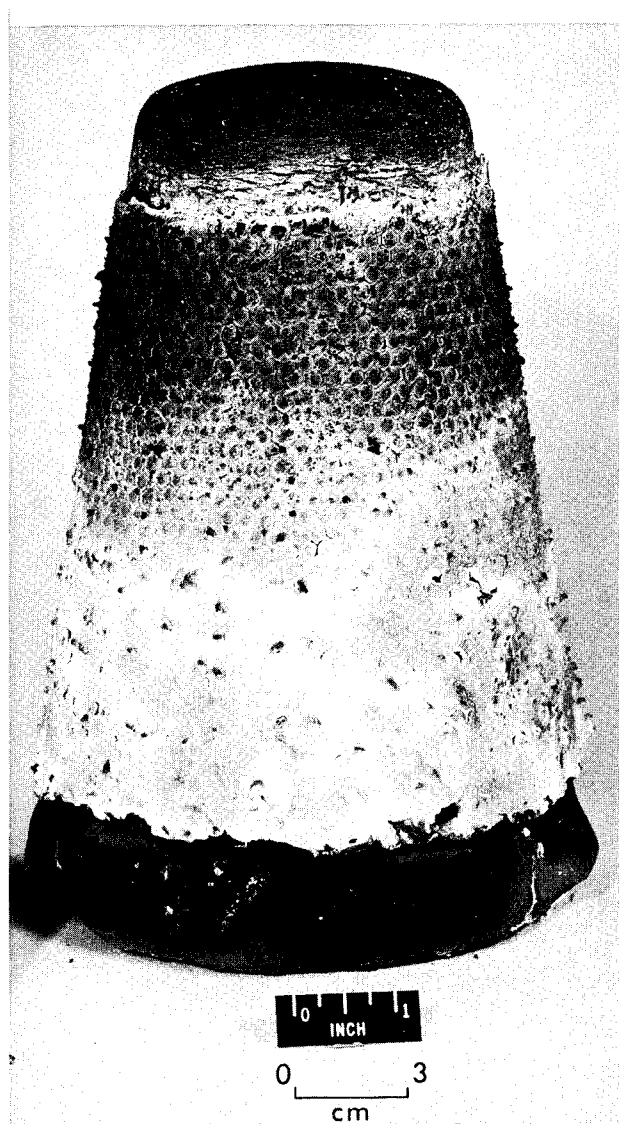
(a) Model 5 in air, trajectory I. L-63-748



(b) Model 6 in nitrogen, trajectory I. L-63-738

Figure 10.- Material B after simulation.

models at the low subsonic velocity of the arc-jet stream; however, higher velocity flow would probably remove this residue. Beneath the residue, the degraded material was hard and tough and formed a rough irregular surface, particularly on the model tested in air. Otherwise, there was little difference in the outward appearance of models 5 and 6. Model 6 had a dark-colored deposit near the nose-cap junction which may have resulted from nose-cap ablation products. In general, the post-test appearance of ablation material B was similar to its post-test appearance on the planar specimens reported in references 3 and 4.

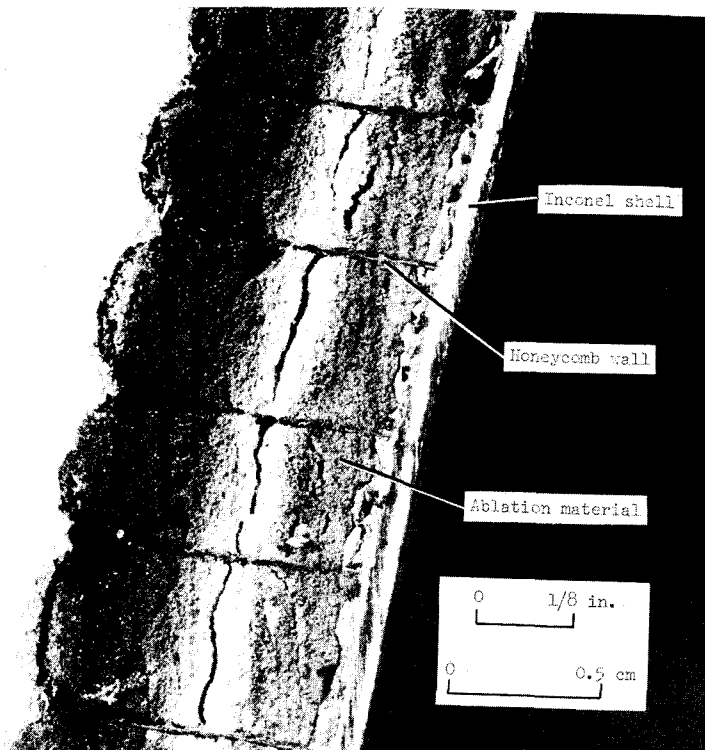


(c) Model 7 in air, trajectory II. L-63-744

Figure 10.- Concluded.

Figure 10(c) shows the post-test appearance of model 7 after exposure to the trajectory II simulation in air. This model developed more severe surface irregularities than models 5 and 6. At the region of highest heating rates, near the nose, the entire thickness of the material was degraded and developed longitudinal cracks after test completion. An attempt to section this model was unsuccessful because the honeycomb containing the degraded material separated from the inconel shell.

Figure 11 shows a section of model 5 near the midlength of the model. The expansion of the ablation material out of the honeycomb cells is evident in the photograph. Separation of the ablation material occurred at the boundary between thermally degraded and undegraded material. It is not known whether this separation occurred during heating or during cooling. If the separation occurred during the period between the first and second heating pulses of trajectory I, it might explain the reduced heat penetration exhibited by material B compared to material A during the second heating pulse.



L-63-1910.1

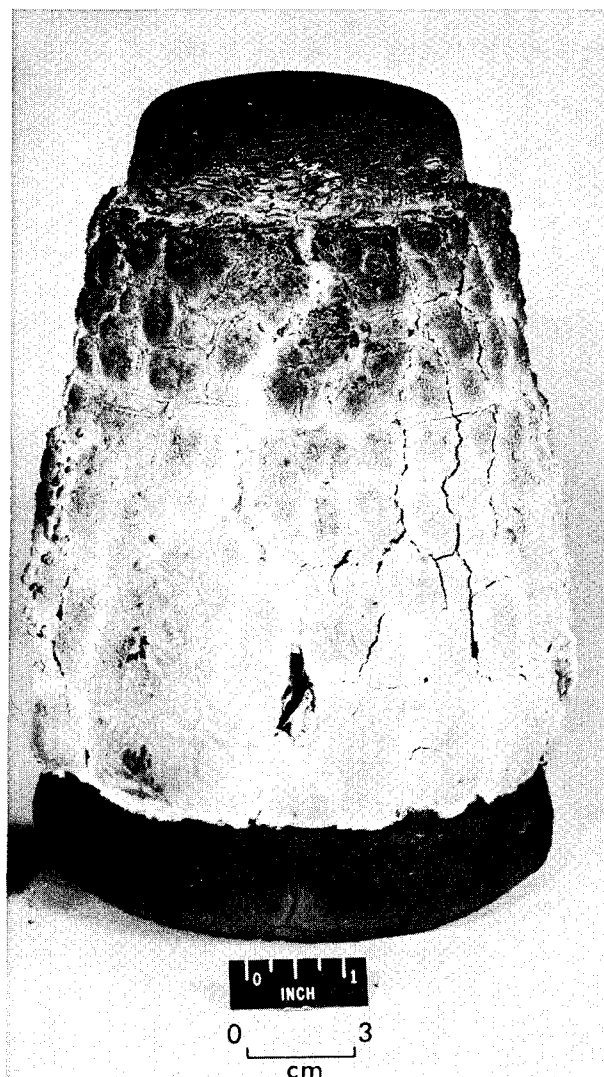
Figure 11.- Section view of material B, model 5, after trajectory I simulation in air.

Material B performed better than material A at the test conditions of this investigation. Material B was able to accommodate the severely restrained thermal expansion without developing the circumferential buckles observed in the tests of material A.

Material C.- The model of material C after exposure to the trajectory II simulation in air is shown in figure 12. The first heat pulse for this test was of longer duration than the other trajectory II simulations because heating-rate measurements made before testing indicated a decrease in the cold-wall heating rate. The reason for the decreased heating rate is not known. The same arc-jet operating conditions were used for all trajectory II simulations. The severe swelling and surface irregularities of the material

are evident in figure 12. The major portion of the swelling occurred during the first heating pulse. Since material C was identical to material B except that no honeycomb reinforcement was used, it appears that the honeycomb substantially reduces the swelling. This model appeared to have longitudinal bulges spaced at approximately equal distances around the model circumference. These bulges are difficult to distinguish in figure 12 because of overall surface irregularity. These bulges also indicate the desirability of using honeycomb reinforcement, since, as previously noted, no bulging or buckling was observed on the material B models. The thermally degraded material on the material C model was weakly attached to the undegraded material and fell off when an attempt was made to section the model. It is probable that much of this degraded material would have been removed in a high-velocity flow.

Although material C was more effective in restricting heat penetration than either of the other materials, problems are indicated in the use of this material without honeycomb reinforcement. The behavior of this material, for the conditions of this investigation, is probably typical of silicone elastomerics. Larger radii, such as on a vehicle afterbody, or less severe restraint might permit the use of unreinforced elastomerics but further testing would be required for verification.



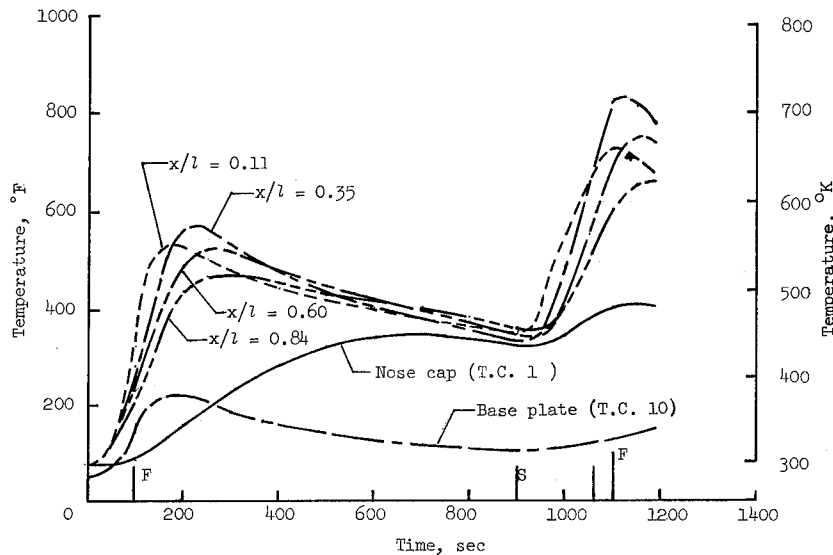
L-63-750

Figure 12.- Material C, model 8 after trajectory II simulation in air.

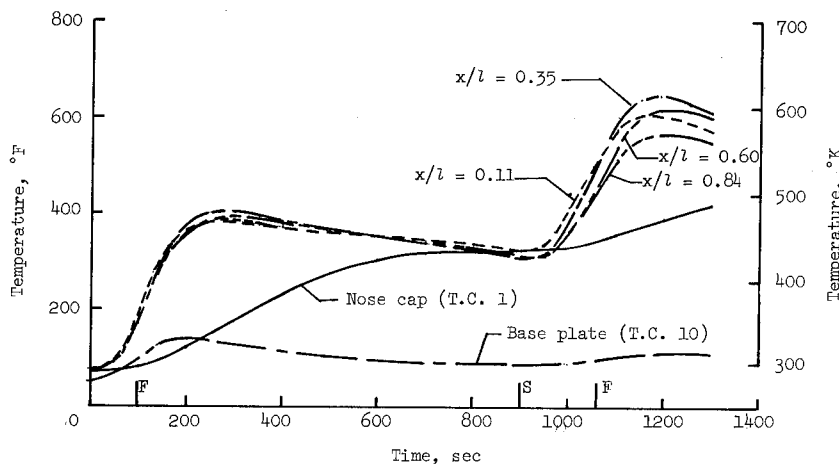
#### Temperature Histories

The model temperature histories are shown in figures 13 to 16. As can be seen from these figures, the inconel cone temperatures reached high values on all models. These temperatures were considerably higher than those used for many ablation-material evaluations. In reference 3, for example, testing was terminated at a temperature of

300° F (422° K). Information available at the time the ablation-material thicknesses were selected for the present investigation indicated that the materials would limit interface temperatures to less than 500° F (533° K) for the heating conditions of these tests. Apparently, the design information used was based on test results obtained at heating rates higher than those of the present investigation. The results of references 3 and 5, which were not available when the models were designed, indicate that ablative effectiveness decreases with decreasing heating rate. The high interface temperatures were



(a) Model 1; air test stream.



(b) Model 2; nitrogen test stream.

Figure 13.- Temperature histories on ablation material A models during trajectory I simulation.

undesirable in that no conclusions concerning bond integrity of ablation material to inconel could be made since the temperature in most tests exceeded the temperature capability of commonly used bonding materials.

Material A.- The temperature histories of the thermocouples on models 1 and 2 which were exposed to the trajectory I simulation are shown in figure 13. The times at which the heating rates were changed and testing terminated are indicated in figure 13. Inasmuch as the thermocouples located  $180^\circ$  apart at the same  $x$  distance on the models (see fig. 2) indicated nearly the same temperature, the temperatures of each pair of thermocouples were averaged and shown in the figures as a single curve. This procedure was followed in preparing the temperature histories for all models except models 3 and 4. The ablation material on models 1 and 2 absorbed a significant quantity of heat as evidenced by the continued temperature rise after the termination of heating. A comparison of the temperature histories in figure 13 shows that the interface temperatures on model 2, tested in nitrogen, were lower than those on model 1 tested in air. The lower temperatures in the nitrogen test were due to a reduced rate of char oxidation at the ablating surface and a correspondingly slower ablation rate. Since the ablation materials tested in this investigation had low values of thermal conductivity, even a slight decrease in the rate of ablation could have a significant effect on the temperatures of the inconel shell.

The temperature histories of the thermocouples on models 3 and 4 which were exposed to the trajectory II simulation are shown in figure 14. Both of these models failed before completion of the test. The interface temperatures on both models reached high values after the ablation material developed severe defects.

Material B.- The temperature histories of the thermocouples on models 5, 6, and 7 are shown in figure 15. Models 5 and 6 were exposed to the trajectory I simulation with arc-jet streams of air and of nitrogen, respectively. The temperature histories for model 1 (fig. 13(a)) and model 5 (fig. 15(a)) show similar interface temperatures at the end of the first heating pulse. However, the peak temperatures for model 5 after the second heating pulse were significantly lower than for model 1 at a corresponding time. The swelling of material B during heating may have decreased the effective thermal conductivity and thus caused a lower temperature response during the second heating period. The previously discussed material separation may also have been a contributing factor.

The temperature histories of model 5 (fig. 15(a)), tested in air, and model 6 (fig. 15(b)), tested in nitrogen, show that the peak temperatures were significantly higher in the airstream and indicate that material B was affected by oxidation. However, a comparison of the temperature histories for model 2 (fig. 13(b)) and model 6 (fig. 15(b)) shows that reducing the test-stream oxygen content and thus reducing the char-layer oxidation decreased the heat penetration in material A more than in material B.

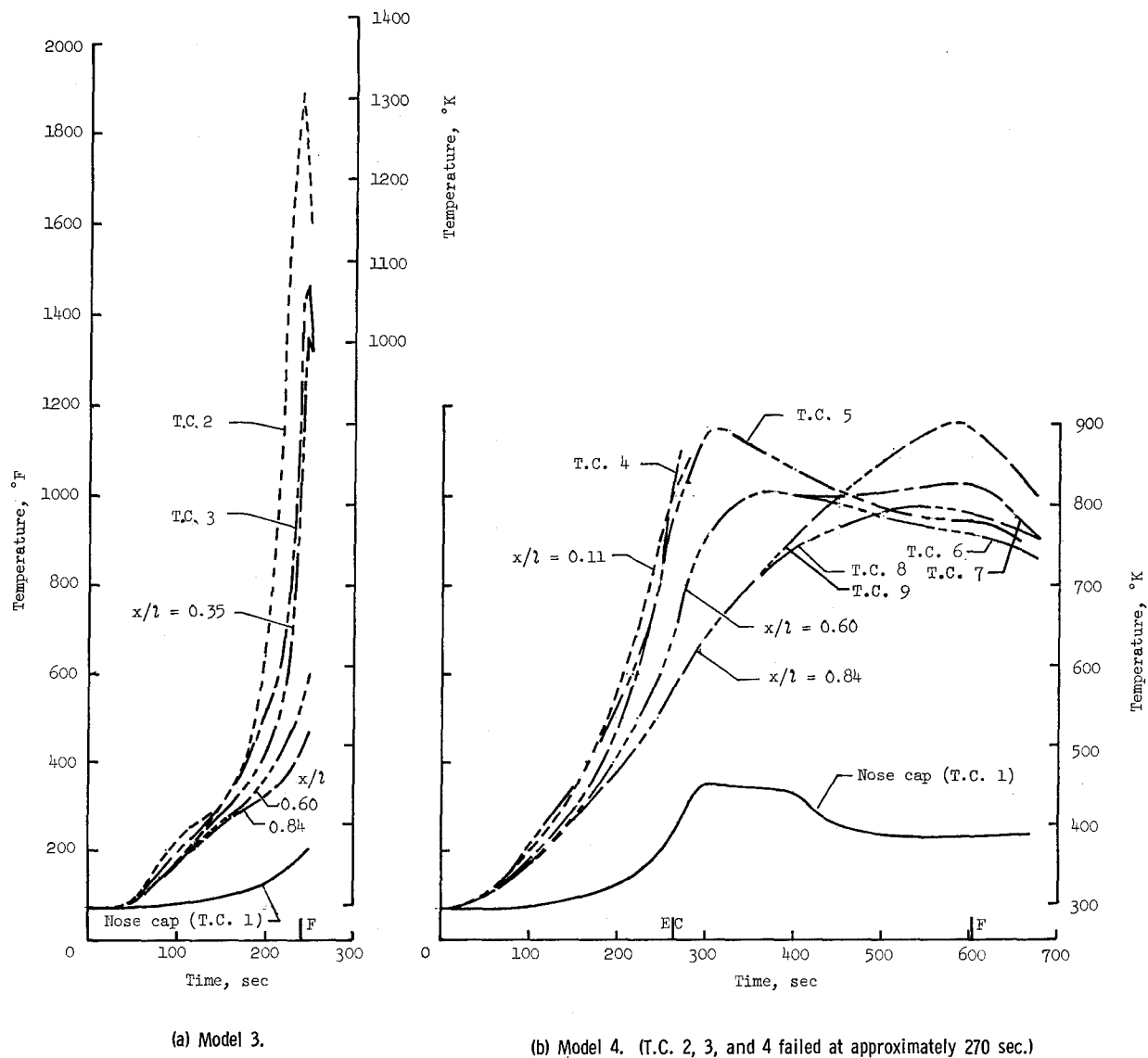
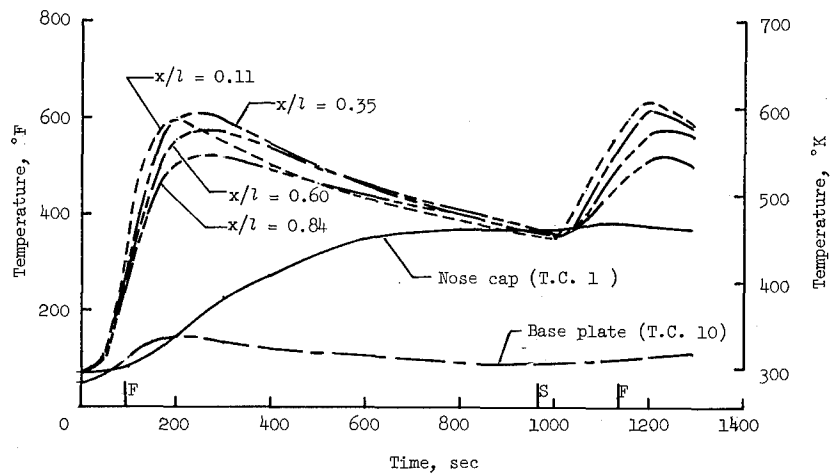
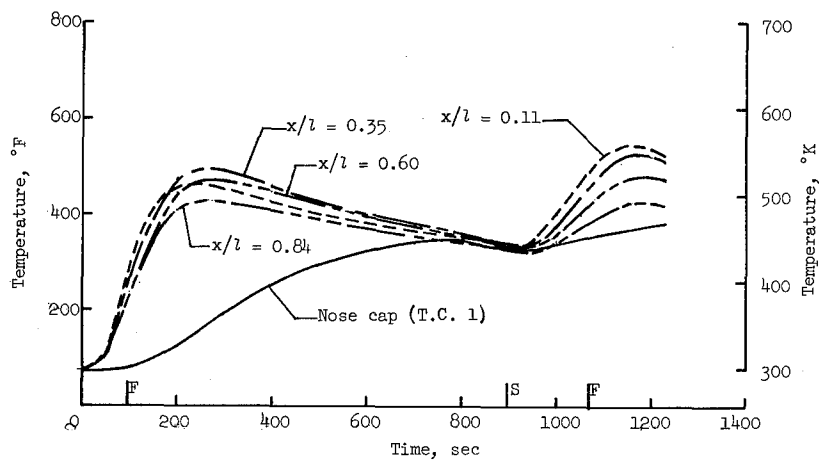


Figure 14.- Temperature histories of thermocouples on ablation material A models during trajectory II simulation in an air test stream. Thermocouple 10 was not operative on these models.

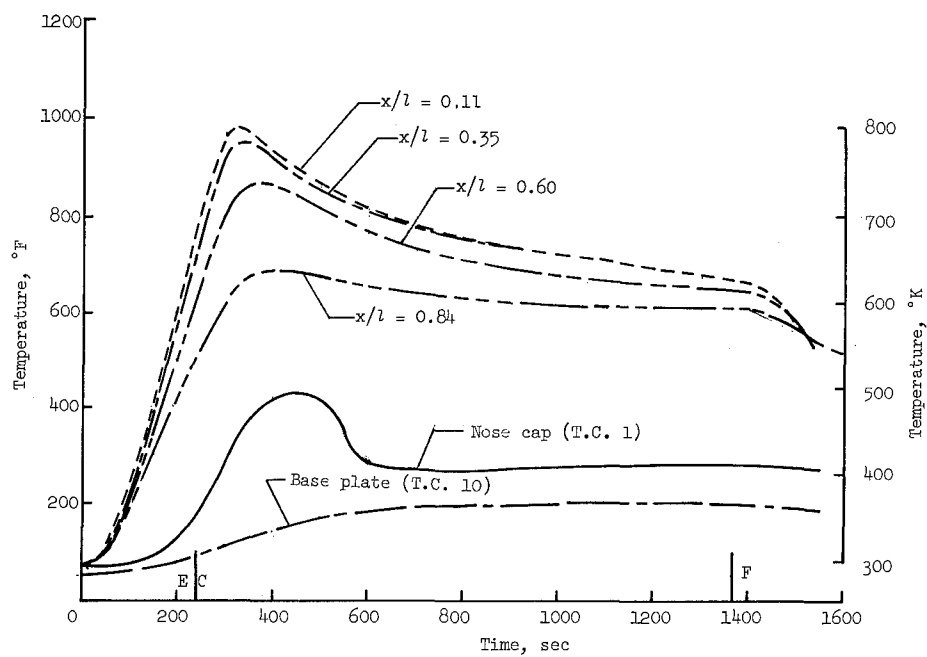


(a) Model 5; trajectory I simulation in air test stream.



(b) Model 6; trajectory I simulation in nitrogen.

Figure 15.- Temperature histories on ablation material B models.



(c) Model 7; trajectory II simulation in air test stream.

Figure 15.- Concluded.

This result was expected since the carbonaceous char layer of ablation materials such as material A is strongly affected by oxidation.

The temperature history of model 7 exposed to trajectory II simulation in air is shown in figure 15(c). The interface temperatures reached high values but the temperatures were considerably lower than for model 3 (fig. 14(a)) which was covered with material A. Also, model 7 remained intact for the entire test whereas models 3 and 4 failed.

Material C.- Figure 16 shows the temperature history of model 8 during exposure to the trajectory II simulation in air. A comparison of figures 15(c) and 16 shows that material C was more effective than material B in restricting heat penetration during the trajectory II simulation. The pronounced swelling of material C during heating and the fact that this material did not have honeycomb reinforcement as did material B probably contributed to its resistance to heat penetration.

Because of heating-rate variations and temperature gradients along the models plus the temperature-equalizing effect of the continuous inconel shell, the temperature histories were not used to calculate the ablative effectiveness of the ablation materials. The test results available for comparison were obtained from planar specimens exposed to one-dimensional heating rather than the two-dimensional heating of the present investigation. The ablative effectiveness of the ablation materials for the test conditions of this investigation was low because the test environment, particularly the trajectory II simulation, caused the material to function primarily as a high-temperature insulator. At the low enthalpy and low heating rate of these tests, the reradiation and ablation mechanisms of heat blockage are less important than the thermal conductivity of the ablation material.

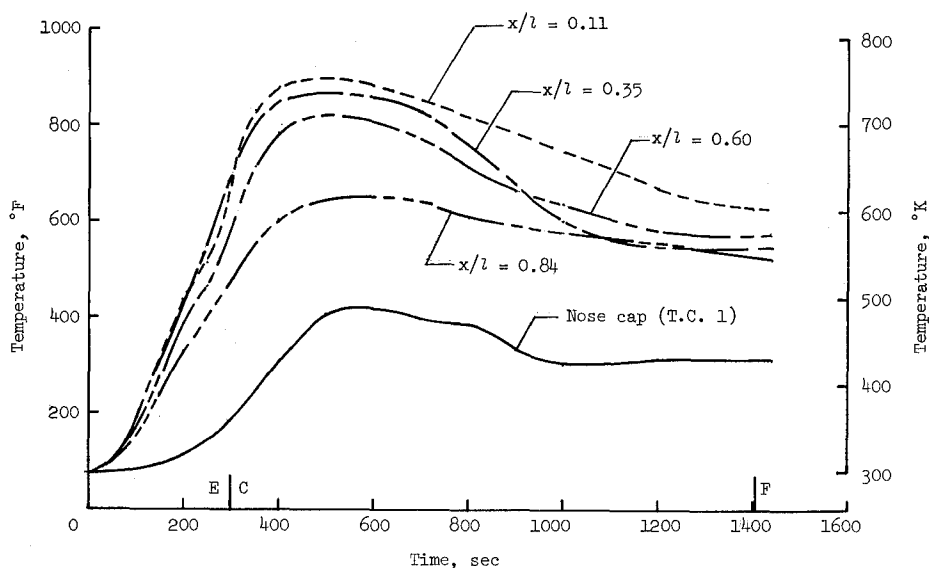


Figure 16.- Temperature history of model 8 (ablation material C) during trajectory II simulation in an air test stream.

## CONCLUDING REMARKS

Eight cone models consisting of a truncated inconel cone and a contoured plastic nose cap with ablation materials bonded to the inconel cone were tested in an arc jet. The test conditions were established from an estimate of the afterbody heating on a lifting vehicle during an overshoot and undershoot reentry. The models were exposed to low heating rates for long times to investigate the ability of several types of ablation material to resist differential thermal expansion, restrained thermal expansion, and heat penetration. Three types of ablation materials were tested: material A, an epoxy-based molded ablator; material B, a silicone elastomeric ablator in honeycomb, and material C, the same as material B without honeycomb. The ablation materials were bonded to the inconel cone in thicknesses corresponding to 1.5 lbm/sq ft ( $7.3 \text{ kg/m}^2$ ). Temperature measurements were made at several locations on the interior of the inconel cone during testing.

The char layer of material A developed "mud flat" crack patterns during testing similar to those reported elsewhere in tests of this material on planar specimens. Unlike the planar specimens, however, the models of this investigation developed severe buckling and two models failed catastrophically during testing. The small size of the cones and the severe restraint to thermal expansion undoubtedly accentuated the buckling behavior of this material. The test results, however, indicated that restrained thermal expansion is a potential problem area in the use of relatively rigid molded ablation materials for vehicle-afterbody thermal protection.

Material B developed surface defects similar to those reported in other investigations of the same material in planar specimens; however, this material did not develop buckles during testing. The effect of the honeycomb in material B was substantiated by the fact that material C, without honeycomb, developed longitudinal buckles. The beneficial effect of the honeycomb was also shown by the greatly reduced swelling of material B compared with material C. The thermally degraded material on the material B models was locked in place by the honeycomb, whereas, the thermally degraded material on the material C model was only weakly attached to the undegraded material. Since the silicone elastomeric in honeycomb withstood the severe conditions of this investigation, restrained thermal expansion of this class of material should present no particular problems for vehicle-afterbody thermal-protection systems.

The tests in air and nitrogen showed that the epoxy-based material was affected more by char-layer oxidation than the silicone elastomeric. Except for tests in nitrogen, the silicone elastomeric showed greater resistance to heat penetration than the epoxy-based material.

The ablative effectiveness of the ablation materials was overestimated during model design, and, therefore, for the test conditions of this investigation, the ablation-material thickness was not sufficient to limit the bond-line temperature within the temperature capability of the bond materials. Because of the high bond-line temperatures, the post-test bond integrity of the ablation materials to the inconel cone could not be determined.

Langley Research Center,  
National Aeronautics and Space Administration,  
Langley Station, Hampton, Va., October 7, 1966,  
124-08-03-18-23.

## APPENDIX

### CONVERSION FACTORS – U.S. CUSTOMARY UNITS TO SI UNITS

The International System of Units (SI) was adopted by the Eleventh General Conference on Weights and Measures, Paris, October 1960 in resolution 12 (ref. 1). Conversion factors required for units used herein are:

Physical quantity	U.S. Customary Unit	Conversion factor (*)	SI Unit
Enthalpy . . . . .	Btu/lbm	$2.32 \times 10^3$	joules/kilogram (J/kg)
Heating rate . . . . .	Btu/ft <sup>2</sup> -sec	$1.135 \times 10^4$	watts/square meter (W/m <sup>2</sup> )
Length . . . . .	in.	$2.54 \times 10^{-2}$	meters (m)
Mass flow . . . . .	lbm/sec	0.45	kilograms/sec (kg/s)
Mass distribution . . .	lbm/ft <sup>2</sup>	4.88	kilograms/square meter (kg/m <sup>2</sup> )
Temperature . . . . .	°R	5/9	degree Kelvin (°K)

\*Multiply value given in U.S. Customary Unit by conversion factor to obtain equivalent value in SI Unit.

Prefixes to indicate multiples of units are:

Prefix	Multiple
centi (c)	$10^{-2}$
kilo (k)	$10^3$
mega (M)	$10^6$

## REFERENCES

1. Mechtly, E. A.: The International System of Units - Physical Constants and Conversion Factors. NASA SP-7012, 1964.
2. Chapman, Andrew J.: An Experimental Evaluation of Three Types of Thermal Protection Materials at Moderate Heating Rates and High Total Heat Loads. NASA TN D-1814, 1963.
3. Clark, Ronald K.: Effect of Environmental Parameters on the Performance of Low-Density Silicone-Resin and Phenolic-Nylon Ablation Materials. NASA TN D-2543, 1965.
4. Dow, Marvin B.; and Brewer, William D.: Performance of Several Ablation Materials Exposed to Low Convective Heating Rates in an Arc-Jet Stream. NASA TN D-2577, 1964.
5. Swann, Robert T.; Dow, Marvin B.; and Tompkins, Stephen S.: Analysis of the Effects of Environmental Conditions on the Performance of Charring Ablators. J. Spacecraft Rockets, vol. 3, no. 1, Jan. 1966, pp. 61-67.

TABLE I.- TEST MATERIALS

Material	Source of ablation material	Trade name	Major constituents	Specific gravity
A	AVCO Corporation	Avcoat 5026-22	Epoxy resin, phenolic-microballoons, and quartz fibers	0.962
B	McDonnell Aircraft Corporation	S-3	White silicone elastomeric and silica spheres in non-metallic honeycomb	0.890
C		D-5	Same as S-3 without honeycomb	0.870

TABLE II.- TEST CONDITIONS

(a) U.S. Customary Units

Model	Ablation material	Trajectory	Arc-jet stream	First heating pulse			Period between heating pulse, sec	Second heating pulse			$Q_{tot}$ from jet, $Btu/ft^2$	$Q_{tot}$ from assumed flight heating curves, $Btu/ft^2$
				$q$ , $Btu/ft^2$ -sec	Time, sec	$Q$ , $Btu/ft^2$		$q$ , $Btu/ft^2$ -sec	Time, sec	$Q$ , $Btu/ft^2$		
1	A	I	Air	26	99	2570	801	5	169	845	3415	3300
2	A	I	N <sub>2</sub>	23	99	2270	802	5	164	820	3090	3300
3	A	II	Air	17	240	4080	None	3			4080	7870
4	A	II	Air	17	264	4500	None	5	336	1000	5500	7870
5	B	I	Air	26	98	2450	868	5	170	850	3390	3300
6	B	I	N <sub>2</sub>	24	99	2360	798	5	172	860	3220	3300
7	B	II	Air	17	264	4500	None	3	1100	3300	7800	7870
8	C	II	Air	15	299	4485	None	3	1103	3309	7794	7870

(b) SI Units

Model	Ablation material	Trajectory	Arc-jet stream	First heating pulse			Period between heating pulse, sec	Second heating pulse			$Q_{tot}$ from jet, $MJ/m^2$	$Q_{tot}$ from assumed flight heating curves, $MJ/m^2$
				$q$ , $kw/m^2$	Time, sec	$Q$ , $MJ/m^2$		$q$ , $kw/m^2$	Time, sec	$Q$ , $MJ/m^2$		
1	A	I	Air	300	99	29	801	57	169	9.6	39	3.8
2	A	I	N <sub>2</sub>	260	99	26	802	57	164	8.3	35	3.8
3	A	II	Air	190	240	46	None				46	9.0
4	A	II	Air	190	264	51	None	34	336	1.1	63	9.0
5	B	I	Air	300	98	29	868	57	170	9.7	39	3.8
6	B	I	N <sub>2</sub>	270	99	27	798	57	172	9.8	37	3.8
7	B	II	Air	190	264	51	None	34	1100	3.8	89	9.0
8	C	II	Air	170	299	51	None	34	1103	3.8	88	9.0

*"The aeronautical and space activities of the United States shall be conducted so as to contribute . . . to the expansion of human knowledge of phenomena in the atmosphere and space. The Administration shall provide for the widest practicable and appropriate dissemination of information concerning its activities and the results thereof."*

—NATIONAL AERONAUTICS AND SPACE ACT OF 1958

## NASA SCIENTIFIC AND TECHNICAL PUBLICATIONS

**TECHNICAL REPORTS:** Scientific and technical information considered important, complete, and a lasting contribution to existing knowledge.

**TECHNICAL NOTES:** Information less broad in scope but nevertheless of importance as a contribution to existing knowledge.

**TECHNICAL MEMORANDUMS:** Information receiving limited distribution because of preliminary data, security classification, or other reasons.

**CONTRACTOR REPORTS:** Technical information generated in connection with a NASA contract or grant and released under NASA auspices.

**TECHNICAL TRANSLATIONS:** Information published in a foreign language considered to merit NASA distribution in English.

**TECHNICAL REPRINTS:** Information derived from NASA activities and initially published in the form of journal articles.

**SPECIAL PUBLICATIONS:** Information derived from or of value to NASA activities but not necessarily reporting the results of individual NASA-programmed scientific efforts. Publications include conference proceedings, monographs, data compilations, handbooks, sourcebooks, and special bibliographies.

*Details on the availability of these publications may be obtained from:*

SCIENTIFIC AND TECHNICAL INFORMATION DIVISION  
NATIONAL AERONAUTICS AND SPACE ADMINISTRATION  
Washington, D.C. 20546